PHYSICA B
CONDENSED MATTER

CrossMark

Indentation size effects in the nano- and micro-hardness of a Fe-based bulk metallic glass

F. Xu *, Y.H. Ding, X.H. Deng, P. Zhang, Z.L. Long

College of Civil Engineering and Mechanics, Xiangtan University, Hunan 411105, China

ARTICLE INFO

ABSTRACT

Hardness of a Fe-based bulk metallic glass (BMG) was evaluated by both atomic force microscopy (AFM) nanoindentation (nano-hardness) and instrumented indentation with a traditional indenter setup (micro-hardness) under different maximum loads at room temperature. The nano-hardness and the micro-hardness were found to be comparable. For both of the indentation methods, indentation size effect (ISE) is detected as increase in hardness with decrease in indentation peak load. It is proposed that strain rate dependent softening, loading history and the lag between free volume creation and mechanical softening should be responsible for the ISE in this BMG. Furthermore, ISE is found to be more significant in AFM nanoindentation than in instrumented indentation. This can be explained by taking into account the effect of exerted peak load and the face angle of the indenter in a qualitative manner.

1. Introduction

In the last decade, mechanical properties of bulk metallic glasses (BMGs) on nano-scale have been motivating extensive researches [1–10]. Recently, microscopic structural and mechanical heterogeneities have been found in CuZr [4], Ti [5], Ni [6], Pd [7] and Zr [8–10] based BMGs. Based on the spatial nano-hardness tests, Wang et al. [11] have quantified the mechanical heterogeneity of $Zr_{64.13}Cu_{15.75}Ni_{10.12}Al_{10}$ BMG, whose plastic strain was reported to be over 160% at room temperature [9], and the extraordinary plasticity was attributed to distinctive micrometer-sized structural heterogeneity (i.e., soft and hard regions). On the other hand, nanoindentation hardness of individual shear bands in BMGs has been investigated by some authors for better understanding of the role of free volume in the phenomenological shear localization in metallic glasses [12–16]. Yoo et al. [13] found that the hardness of the shear bands, whose thickness was reported in the range of hundreds of nanometers, is much lower than the respective hardness of undeformed region. From the above mentioned, we can see as the interests in exploring mechanical properties of small samples have increased, indentation techniques should be employed on an even finer scale in order to match the imprint size to the object dimensions. To fulfill this aim, atomic force microscopy (AFM) nanoindentation [17] which has been claimed to be able to extract quantitative mechanical information coupled with its inherently high spatial resolution of imaging, may be a powerful tool to characterize nanoscale properties of BMGs. The prior scanning of the surface with AFM allows one to select areas of interest [18]. Nowadays, this technique has been extensively employed to evaluate hardness on the nanometer scale in a variety of materials [18–21], but its application on BMGs, to the best of our knowledge, is still an open issue.

During the indentation, the most interesting phenomenon is the indentation size effect (ISE) [22,23], which is manifested as an increase in hardness H with decreasing indentation peak load P_{max}. Normally, ISE is not expected to occur in BMGs due to the absence of dislocations and strain hardening. However, in some investigations ISE was reported in Zr [24–26], Pd [27], Au-based BMGs [28] and amorphous solids [22]. The strain-induced softening due to the excessive free volume creation during plastic deformation was regarded as the main cause for ISE [24]. To date, the reported ISE in BMGs are mainly studied by instrumented indentation on the micrometer scale (with the peak load of ∼ mN). Therefore, it is intriguing to know whether and how ISE would exist on a nanometer scale under AFM nanoindentation, as the possible mechanisms causing the ISE may play a key role on better understanding of the plastic deformation in BMGs.

With this in mind, we performed AFM nanoindentation and instrumented indentation tests to evaluate the hardness of exactly the same $(Fe_{0.432}Co_{0.288}B_{0.192}Si_{0.048}Nb_{0.04})_{96}Cr_4$ BMG [29] samples at room temperature. The results show that the hardness values obtained from AFM nanoindentation are comparable to those

* Corresponding author. Tel.: +86 731 58293861.
 E-mail address: xufu@xtu.edu.cn (F. Xu).

obtained from instrumented indentation. ISE behaviors clearly exist in the studied BMG not only on micrometer scale but also on nanometer scale. ISE is more significant in AFM nanoindentation than in instrumented indentation. This variation and the possible mechanism of ISE in BMGs are discussed.

2. Experiments

BMG with nominal composition $(Fe_{0.432}Co_{0.288}B_{0.192}Si_{0.048}Nb_{0.04})_{98}$ Cr_2 (Fe-based BMG for short in this work) was chosen for this study. Cylindrical rods of 3 mm diameter and 40 mm in length were fabricated by copper mold casting. The amorphous structure of the alloy was ascertained by X-ray diffraction with Cu $K\alpha$ radiation (see Ref. [29]).

Instrumented indentation tests were conducted using a tribo-Indenter from Hysitron Inc. with a standard Berkovich diamond indenter. Experiments at constant loading rates of 2 mN s^{-1} were carried out to the load limit of 50, 100, 150 and 200 mN. At least six indentation tests were carried out under each condition. AFM nanoindentation test was carried out using an AFM (NanoscopeIII Dimension 3100, DI) equipped with a diamond tip mounted on a stainless cantilever. Sensitivity of the cantilever calibrated on sapphire sample before and after indentation tests was 95 nm V^{-1} with a spring constant of about 235 N m^{-1}. Tip geometry of the indenter consists of a sharp three-sided pyramid, the base of which was an equilateral triangle with a half angle of $30 \pm 2°$. The radius of curvature at the tip apex was nominally less than 20 nm. The frequency of the indentation cycle for AFM nanoindentation was set to be 1.0 Hz (one loading/unloading cycle per second). The trigger thresholds were set ranging from 0.5 to 2.0 V with value increment of 0.5 V, which corresponds to different peak loads from 11.15 to 44.60 μN. Prior to all the indentation experiments, the BMG cylindrical rods were cut into 5 mm thick cylinders and the surface of samples was carefully polished to a mirror finish to ensure a mean roughness of less than 5 nm. The AFM images were obtained with the same indenter used in AFM nanoindentation.

3. Results

Fig. 1 shows the representative load-depth (P–h) curves from instrumented indentation experiments. The loading portion of the (P–h) curves obtained at different P_{max} overlapped one another perfectly, proving that the tests are remarkably reproducible.

The advantage of instrumented indentation technique is that the hardness can be evaluated by only (P–h) curve analysis, without observation of the residual indentation impression. The most popular way to perform this analysis is the Oliver–Pharr [30] (O–P) method. However, we do not follow this way in the present work. One reason is that severe material pile-up is usually observed around the indentation impression in BMGs, and such pile-up is often dismissed in the O–P method, which induces an overestimation of the calculated hardness. From the post-mortem topographies after the sample was indented at P_{max} of 50 mN (Fig. 1(a)) and 200 mN (Fig. 1(b)), high and extended pile-up can be observed. It is also revealed in Fig. 2 that the ratio of the pile-up height ($h_{pile-up}$) to the maximum residual depth (h_{res}) increased with reducing peak load which agrees with the results of Charleux et al. [31,32] and Jang et al. [25].

As pointed out by Jang et al. [25], the overestimation of hardness induced by pile-up will be more apparent at smaller depth, which may raise doubt about whether the ISE-like trend is an artifact or not. Another reason why we desert the O–P method is that the correlation constant β (which relates stiffness S to area A) cannot be obtained for the indenter used in AFM

nanoindentation. Furthermore, it is hard to get the unloading stiffness precisely from the unloading segment of (P–h) curves of AFM nanoindentation. In order to overcome these difficulties and obtain accurate hardness, the method used by Jang et al. [25] to explore the ISE in BMGs is adopted in the present work. They measured the impression size A directly from a large number of SEM images (AFM images for our work) and obtained the hardness according to the relation

$$H = \frac{4P}{3\sqrt{3}a^2} \tag{1}$$

where a is the averaged length measured from the center of the triangular impression to the corner.

Surface morphology before and immediately after the accomplishment of AFM nanoindentation is shown in Fig. 3(a) and (b). In Fig. 3(b), significant material pile-up near the nanometer-scale triangular indents from the left to the right (44.60–11.15 μN) is observed. The size and morphology of the indents by the same P_{max} are nearly uniform, indicating the reproductivity and stability of the tests. For clarity, a 3D surface plot of the selected area of Fig. 3(b) is provided in Fig. 3(c). In light of the method mentioned above for handling the pile-up in instrumented indentation, $h_{pile-up}/h_{res}$ vs. P_{max} curve of AFM nanoindentation can also be found in Fig. 2. $h_{pile-up}$ here is the average of three pile-up height values of a triangular indent because the pile-up phenomenon is not as unique as that in instrumented indentation by comparing Fig. 1(a) and (b) with Fig. 3(b). It is also demonstrated in Fig. 2 that $h_{pile-up}/h_{res}$ for AFM nanoindentation decreases with the increasing P_{max}, with exactly the same trend as that for instrumented indentation. It should be well noted that $h_{pile-up}/h_{res}$ is much larger in AFM nanoindentation (2.176–0.939) than that in instrumented indentation (0.257–0.163). The difference can be ascribed to the fact that a sharper indenter and smaller P_{max} are utilized in AFM nanoindentation, which will cause a more pronounced pile-up as reported in Refs. [25] and [31,32]. Furthermore, the great value of $h_{pile-up}/h_{res}$ for AFM nanoindentation reminds us again that the O–P method may not be appropriate to calculate hardness in this study. Enlarged AFM images of two representative indents corresponding to indentation P_{max} of 22.30 and 44.60 μN (circled in Fig. 3(c)) with numbers of 1 and 2, respectively) are shown in Fig. 3(d). Regular triangular indents with clear boundaries can be observed. The same topography has been shown in Fig. 1 for instrumented indentation.

According to Eq. (1), hardness of Fe-based BMG is calculated by measuring the impression size from AFM images. The variation in hardness summarized as a function of P_{max} is shown in Fig. 4(a).

The hardness determined by instrumented indentation is 11.51–12.51 GPa. Since yield strength σ_y of the selected BMG has been verified to be ~4.0 GPa [29], the value is reasonable considering the relation $H \approx 3\sigma_y$ ($H \approx 12.0$ GPa) [33]. On the other hand, hardness measured by AFM nanoindentation (9.98–13.07 GPa) agrees well with that obtained by instrumented indentation. We thus conclude that, for the Fe-based BMG, reliable hardness value can be obtained by AFM nanoindentation with P_{max} chosen in the present work. From Fig. 4(a), the ISE is clearly observed in both indentations.

Following empirical Meyer equation, a power law to describe the scale dependence of the hardness was proposed by Milman et al. [23], which is shown below

$$H = KP_{max}^n \tag{2}$$

where K is a constant, and $n < 0$, i.e. the hardness H decreases as the peak load P_{max} increases. It had been verified that Eq. (2) can be used for single crystals and polycrystals, if the size of the hardness indent is smaller than the grain size. Because ISE was observed for both used indentation modes, we have attempted to
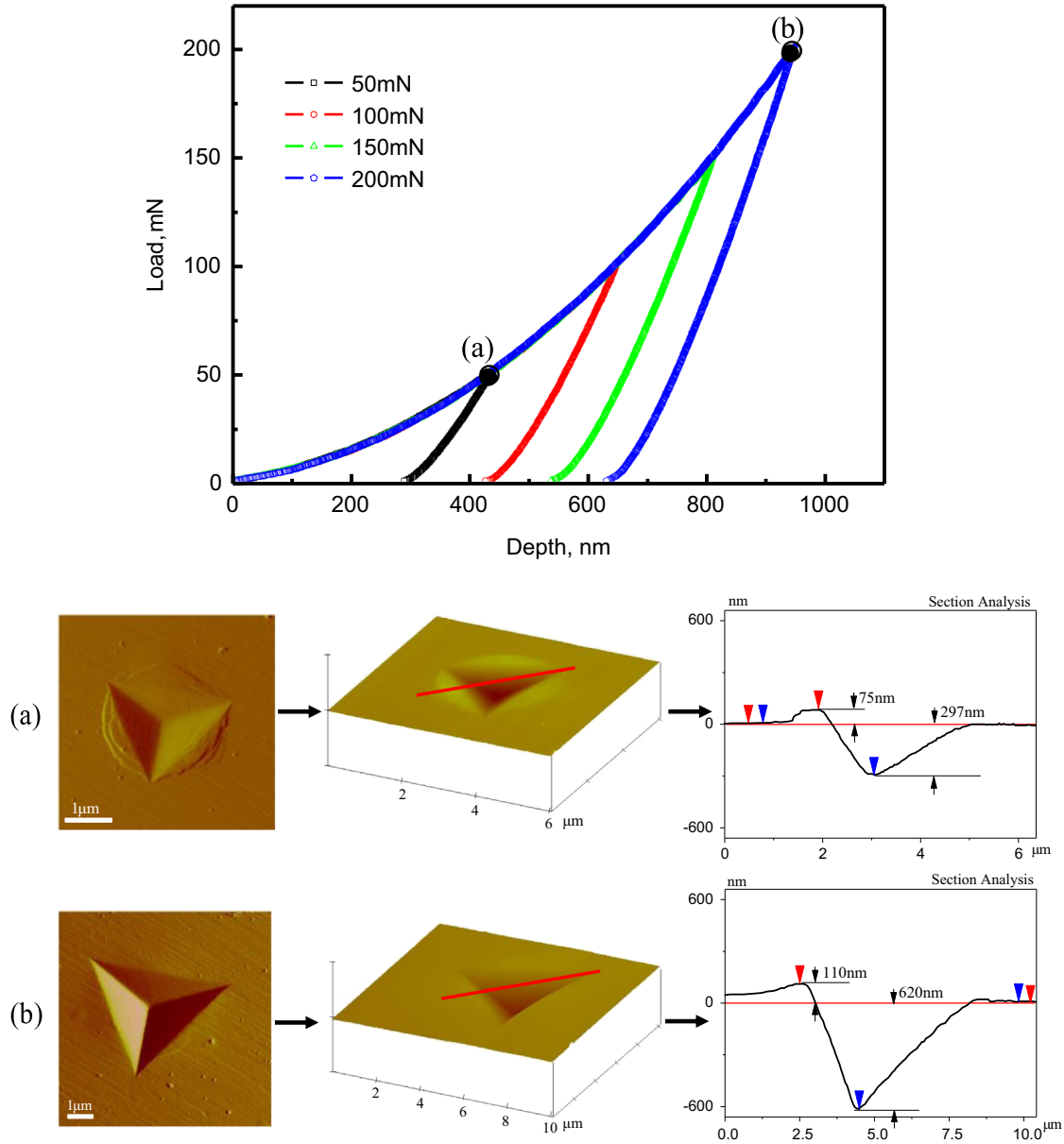
Fig. 1. Instrumented indentation load vs. depth curves at different maximum loads. The insets show the AFM topology and section of residual imprint on the sample after loading at 50 mN (a) and 200 mN (b).

examine whether the ISE could be described according to Eq. (2). The dependence of the hardness on the maximum load in a double-logarithmic coordinates is shown in Fig. 4(b). Surprisingly, a good linearity between $\log H$ and $\log P_{max}$ is seen in both indentations. In fact, similar behavior of a Zr-BMG has been depicted in previous work [26], but without using Eq. (2). Usually, the power law exponent n in Eq. (2), which corresponds to the slope of the fitted line, can characterize the ISE quantitatively. From Fig. 4(b), we find $n = -0.066$ in instrumented indentation and $n = -0.194$ in AFM nanoindentation, respectively. This suggests that ISE is more pronounced in AFM nanoindentation than in instrumented indentation.

4. Discussion

It has been reported that flow events in metallic glasses are accompanied by dilatation, i.e. the creation of free volume [34–37].

In metallic glasses, a certain concentration of flow defects c_f inherently exists. During plastic flow at low homologous temperature, the defect concentration increases. The evolution of the defect concentration $c_f(t)$ is taken as [36]

$$\dot{c}_f(t) = a_x \dot{\varepsilon}(t) c_f(t) \ln^2 c_f(t) \tag{3}$$

with a_x a temperature-dependent parameter and $\dot{\varepsilon}(t)$ the strain rate during indentation. Hence, the production of free volume during plastic flow is proportional to the strain rate and the concentration of pre-existing flow defects in the sample.
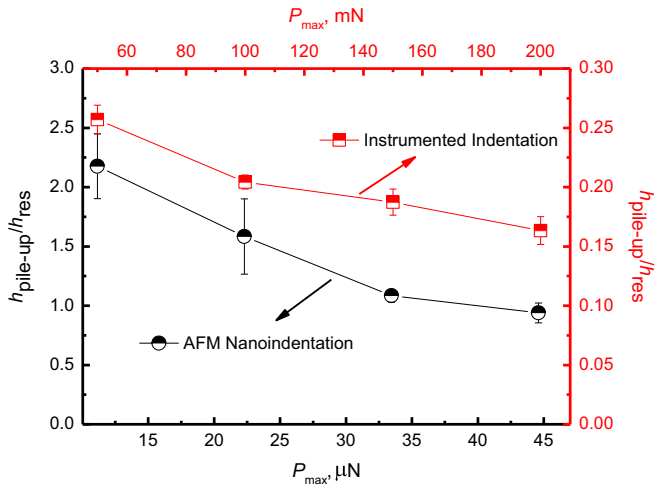
It is well known that for any elastic–plastic materials under a sharp indentation, the loading curve can be described as

$$P(t) = Ch^m(t) \tag{4}$$

where C and m are constants related to the material properties. The strain rate during indentation can be calculated as $\dot{\varepsilon}(t) = \dot{h}(t)/h(t)$, thus for indentation under constant loading rate k (as

$P(t) = kt)$, $\dot{\varepsilon}(t)$ can be expressed as

$$\dot{\varepsilon}(t) = (k/C)^{1/m}\frac{1}{m}(t)^{1/m-1}\frac{1}{(k/C)^{1/m}t^{1/m}} = \frac{1}{mt} \qquad (5)$$

Fig. 2. Variation in the ratio of the pile-up height ($h_{pile-up}$) to the maximum residual depth (h_{res}) as a function of P_{max} (top x and right y for instrumented indentation, bottom x and left y for AFM nanoindentation, respectively).

According to Spaepen [34] and Argon [35], the flow equation that governs the shear strain rate in metallic glasses can be written as

$$\dot{\gamma}(t) = 2c_f(t)\alpha_0 k_{f,0}\frac{\varepsilon_0 v_0}{\Omega}\sinh\left(\frac{\tau\varepsilon_0 v_0}{2k_BT}\right)\exp\left(\frac{-\Delta G}{k_BT}\right) \qquad (6)$$

Based on the classical metallic glasses flow equation developed by Spaepen and Argon, Van Steenberge et al. [24] proposed a relationship between the hardness and the strain rate

$$H(\approx 3\sqrt{3}\tau) \propto \sinh^{-1}\left(\frac{\alpha\dot{\gamma}}{c_f}\right) \qquad (7)$$

where τ is the shear stress, α is a constant, and $\dot{\gamma}$ is the shear strain rate proportional to the strain rate as $\dot{\varepsilon} = \dot{h}/h$. Note that the indentation function of Van Steenberge et al. [24] consists of a loading segment of 40 s at a different P_{max}. This loading mode corresponds to a higher $\dot{\varepsilon}$ for a smaller P_{max} at an arbitrary h during indentation loading process, although all $\dot{\varepsilon}$ values tend to be constant eventually, as can be seen from Fig. 4 in Ref. [24]. According to Eq. (3), the production of free volume will be more pronounced for larger P_{max}, and ISE thus will be observed based on relation (4)–(7).

The strain softening caused by the continuous accumulation of excess free volume during deformation has been successfully utilized for explaining ISE in metallic glasses [24,27,28], which
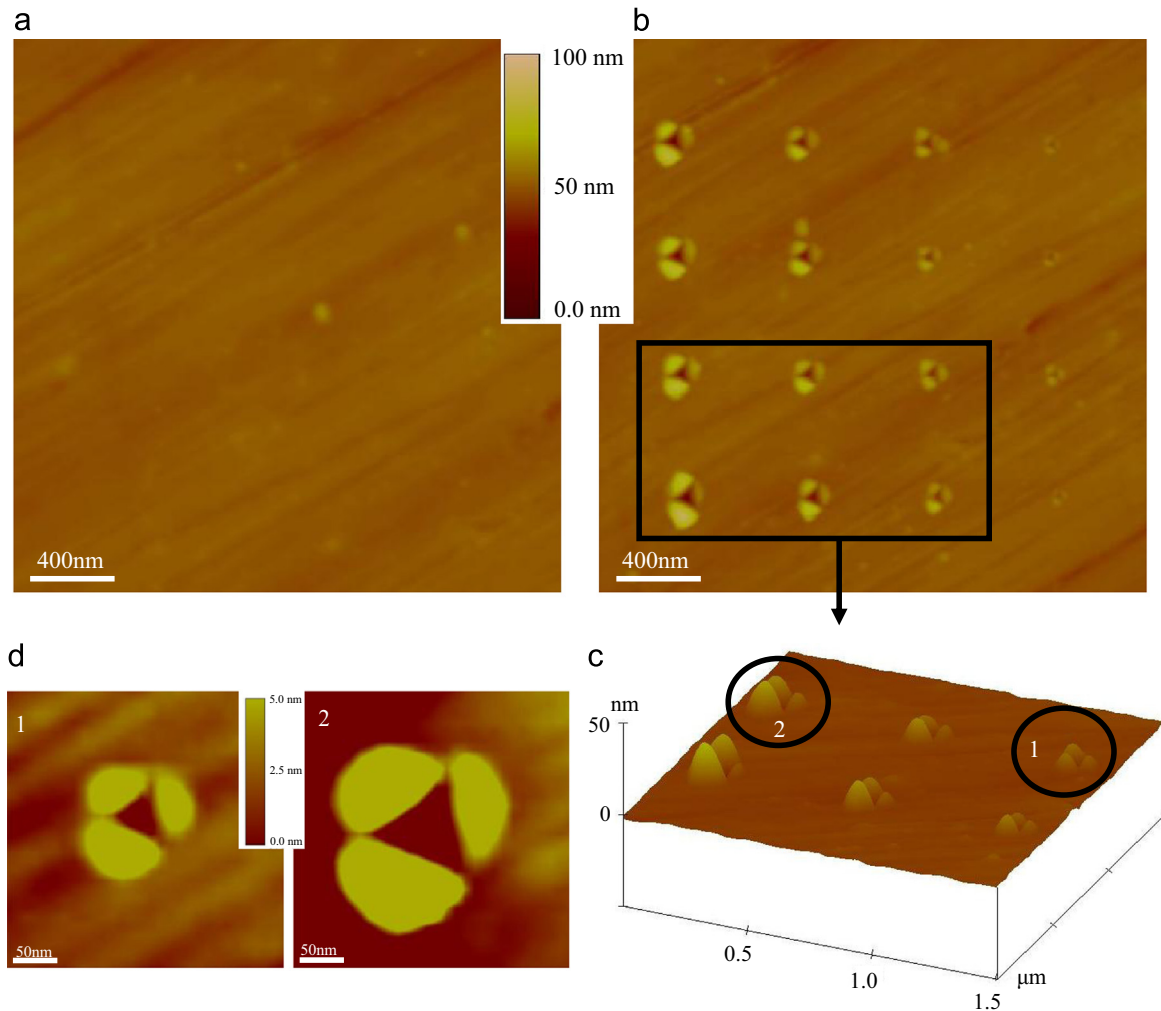
Fig. 3. Matrix of 4×4 AFM nanoindentation results of the Fe-based BMG: (a) image before indentation; (b) image after indentation and P_{max} increasing from 11.15 to 44.60 µN (from the upper-right indentation to the lower-left one, respectively); (c) topographical AFM image of the selected area in (b); (d) enlarged AFM images of the indents circled in (c). (1) P_{max}=22.30 µN and (2) P_{max}=44.60 µN)
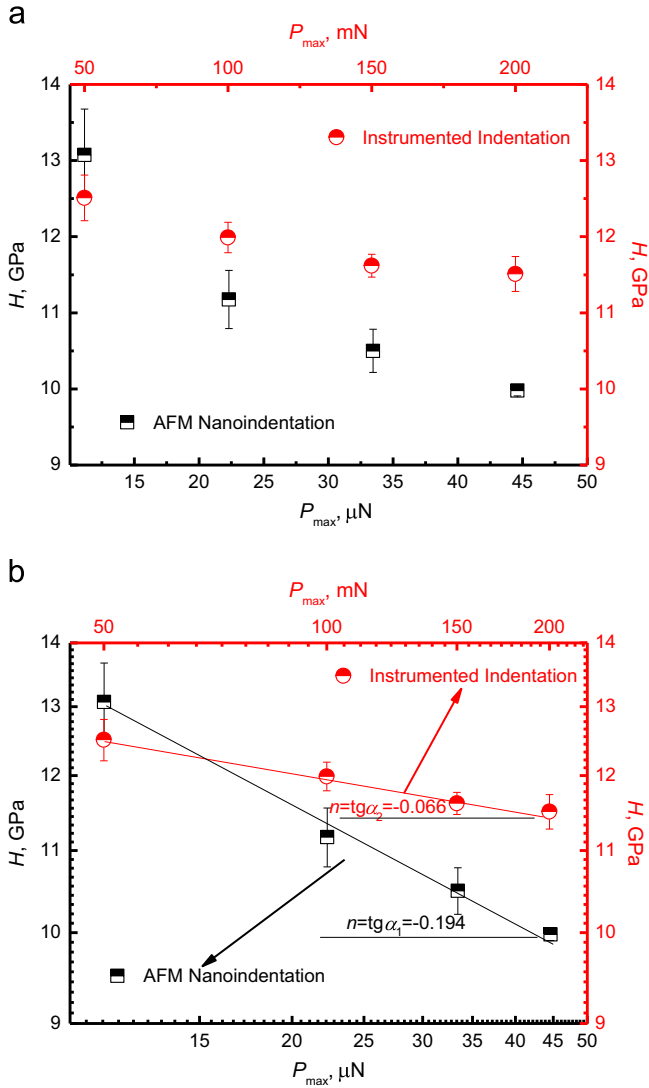
Fig. 4. Dependence of the hardness on the indentation load (top *x* and right *y* for instrumented indentation, bottom *x* and left *y* for AFM nanoindentation): (a) in linear coordinates and (b) in double-logarithmic coordinates.

recently has been excluded by Jang et al. [25], who has performed indentation experiments under a constant strain rate ($0.05\ \text{s}^{-1}$) instead of a constant loading time to explore the main cause of the observed ISE in a Zr-based BMG. They argued that as the indentation strain rate was kept constant, ISE was not expected to occur. In present work, a constant loading rate ($2\ \text{mN s}^{-1}$) is used for instrumented indentation. Hence for different P_{max}, the indentation strain rate will also be the same at a certain h, resulting in the absence of ISE, which is not consistent with the experimental phenomenon. Nevertheless, we here still rely on the strain softening mechanism developed by Vansteenberge et al. [24] for the reasons as below.

The production of free volume during plastic flow is proportional to not only the strain rate, but also the concentration of pre-existing flow defects in the sample. According to Eq. (3), the defects concentration c_f continues to increase as long as the plastic flow $\dot{\varepsilon} > 0$ [38]. If we take into account the numerical integration of Eq. (3) (although it cannot be calculated here due to the absence of proper parameters such as α_x, etc.) with the applicable initial value of c_f, we may find at least that the amount of defect creation will also depend on the experimental time. During indentation under constant strain rate (Jang et al. [25]) or constant loading rate

(instrumented indentation in our work), the higher the applied P_{max} is, the longer the time is needed to reach P_{max}, thus a larger amount of free volume will be accumulated considering the numerical integration of Eq. (3).

On the other hand, the mechanical softening associated with the deformation induced creation of free volume is not necessarily instantaneous. In fact, the time-dependent deformation behavior has been reported during indentation [39–42] and uniaxial compression [43,44] of BMGs at room temperature. Therefore in indentation test without holding period, the generated free volume during the early stage of loading may have an effect on the mechanical softening behavior of following loading segment. In other words, to accommodate the excess free volume generated previously, indentation with increasing load will continue to soften over time. Furthermore, the increased defect concentration will accelerate the following free volume creation process according to Eq. (3). Thus considering the loading history coupled with the lag between free volume creation and mechanical softening (i.e. the dynamic property of softening), more free volume will be accumulated for indentation with greater peak load which need more time to reach P_{max}, which yields the observed ISE.

For AFM nanoindentation in the present work, the frequency of the indentation cycle was set to be 1.0 Hz. Hence the greater the peak load is, the higher the strain rate would be. Thus the mechanism based on strain rate dependent mechanical softening is sound for the explanation of ISE. Moreover, as suggested by Jang et al. [25], the occurrence of STZs might be controlled by the indentation size or the volume of the indentation-induced elastic/plastic deformation. The higher hardness might be observed in the shallow indentation using a sharper indenter with a smaller centerline-to-face angle θ. This is because the highly stressed volume beneath the indenter is too small to have a sufficient population of STZs and thus the glass was required to shear in particular locations. The θ of the AFM indenter, about 30°, is smaller than that of the instrumented indenter, about 65.3°. Therefore, the ultra-low load together with the angle effect on hardness may contribute to the more pronounced ISE in AFM nanoindentation observed in the present work, as shown in Fig. 4.

5. Conclusions

Nano- and micro-hardness of $(Fe_{0.432}Co_{0.288}B_{0.192}Si_{0.048}Nb_{0.04})_{98}Cr_2$ BMG were quantified by AFM nanoindentation and instrumented indentation under different maximum loads at room temperature. The nano-hardness and the micro-hardness were found to be comparable. Under both indentation modes, ISE manifested as increase in hardness H with decreasing indentation peak load P_{max}. Strain rate dependent softening caused by the continuous accumulation of excess free volume during deformation, together with the loading history and the lag between free volume creation and mechanical softening, are proposed to be responsible for the ISE in BMG. In the AFM nanoindentation, the ISE is found to be more significant than in instrumented indentation, which is ascribed to the relatively lower P_{max} and sharper indenter.

References

[1] R. Vaidyanathan, M. Dao, G. Ravichandran, S. Suresh, Acta Mater. 49 (2001) 3781.
[2] A. Greer, A. Castellero, S. Madge, I. Walker, J. Wilde, Mater. Sci. Eng. A 375–377 (2004) 1182.
[3] T. Ichitsubo, S. Hosokawa, K. Matsuda, E. Matsubara, N. Nishiyama, S. Tsutsui, A.Q.R. Baron, Phys. Rev. B 76 (2007) 140201.
[4] J. Das, M.B. Tang, K.B. Kim, R. Theissmann, F. Baier, W.H. Wang, J. Eckert, Phys. Rev. Lett. 94 (2005) 205501.
[5] B.J. Park, H.J. Chang, D.H. Kim, W.T. Kim, K. Chattopadhyay, T.A. Abinandanan, S. Bhattacharyya, Phys. Rev. Lett. 96 (2006) 245503.
[6] A. Concustell, N. Mattern, H. Wendrock, U. Kuehn, A. Gebert, J. Eckert, A. Greer, J. Sort, M. Baro, Scr. Mater. 56 (2007) 85.
[7] H. Wagner, D. Bedorf, S. Küchemann, M. Schwabe, B. Zhang, W. Arnold, K. Samwer, Nat. Mater. 10 (2011) 439.
[8] X.H. Du, J.C. Huang, K.C. Hsieh, Y.H. Lai, H.M. Chen, J.S.C. Jang, P.K. Liaw, Appl. Phys. Lett. 91 (2007) 131901.
[9] Y.H. Liu, G. Wang, R.J. Wang, D.Q. Zhao, M.X. Pan, W.H. Wang, Science 315 (2007) 1385.
[10] Y.H. Liu, D. Wang, K. Nakajima, W. Zhang, A. Hirata, T. Nishi, A. Inoue, M. W. Chen, Phys. Rev. Lett. 106 (2011) 125504.
[11] J.G. Wang, D.Q. Zhao, M.X. Pan, C.H. Shek, W.H. Wang, Appl. Phys. Lett. 94 (2009) 031904.
[12] B.-G. Yoo, K.-W. Park, J.-C. Lee, U. Ramamurty, J.-I. Jang, J. Mater. Res. 24 (2009) 1405.
[13] B.-G. Yoo, Y.-J. Kim, J.-H. Oh, U. Ramamurty, J.-I. Jang, Scr. Mater. 61 (2009) 951.
[14] B.-G. Yoo, J.-Y. Kim, Y.-J. Kim, I.-C. Choi, S. Shim, T.Y. Tsui, H. Bei, U. Ramamurty, J.-I. Jang, Int. J. Plast. 37 (2012) 108.
[15] I.-C. Choi, Y.-J. Kim, Y.M. Wang, U. Ramamurty, J.-I. Jang, Acta Mater. 61 (2013) 7313.
[16] I.-C. Choi, Y. Zhao, Y.-J. Kim, B.-G. Yoo, J.-Y. Suh, U. Ramamurty, J.-I. Jang, Acta Mater. 60 (2012) 6862.
[17] B. Bhushan, V.N. Koinkar, Appl. Phys. Lett. 64 (1994) 1653.
[18] F. Sansoz, T. Gang, Ultramicroscopy 111 (2010) 11.
[19] H. Zhang, J. Tang, L. Zhang, B. An, L.-C. Qin, Appl. Phys. Lett. 92 (2008) 173121.
[20] X. Li, H. Gao, C.J. Murphy, L. Gou, Nano Lett. 4 (2004) 1903.
[21] S.N. Dub, Y.Y. Lim, M.M. Chaudhri, J. Appl. Phys. 107 (2010) 043510.
[22] I. Manika, J. Maniks, Acta Mater. 54 (2006) 2049.
[23] Y.V. Milman, A.A. Golubenko, S.N. Dub, Acta Mater. 59 (2011) 7480.
[24] N. Vansteenberge, J. Sort, A. Concustell, J. Das, S. Scudino, S. Surinach, J. Eckert, M. Baro, Scr. Mater. 56 (2007) 605.
[25] J.-I. Jang, B.-G. Yoo, Y.-J. Kim, J.-H. Oh, I.-C. Choi, H. Bei, Scr. Mater. 64 (2011) 753.
[26] F. Yang, K. Geng, P. Liaw, G. Fan, H. Choo, Acta Mater. 55 (2007) 321.
[27] N. Li, K.C. Chan, L. Liu, J. Phys. D: Appl. Phys. 41 (2008) 155415.
[28] N. Li, L. Liu, K.C. Chan, Q. Chen, J. Pan, Intermetallics 17 (2009) 227.
[29] Z.L. Long, Y. Shao, G.Q. Xie, P. Zhang, B.L. Shen, A. Inoue, J. Alloys Compd. 462 (2008) 52.
[30] W.C. Oliver, G.M. Pharr, J. Mater. Res. 7 (1992) 1564.
[31] L. Charleux, S. Gravier, M. Verdier, M. Fivel, J.J. Blandin, J. Mater. Res. 22 (2007) 525.
[32] L. Charleux, S. Gravier, M. Verdier, M. Fivel, J.J. Blandin, Mater. Sci. Eng. A 483–484 (2008) 652.
[33] D. Pan, A. Inoue, T. Sakurai, M.W. Chen, Proc. Natl. Acad. Sci. USA 105 (2008) 14769.
[34] F. Spaepen, Acta Metall. 25 (1977) 407.
[35] A.S. Argon, Acta Metall. 27 (1979) 47.
[36] P. de Hey, J. Sietsma, A. van den Beukel, Acta Mater. 46 (1998) 5873.
[37] M. Heggen, F. Spaepen, M. Feuerbacher, J. Appl. Phys. 97 (2005) 033506.
[38] L. Anand, C. Su, Acta Mater. 55 (2007) 3735.
[39] A. Concustell, J. Sort, A.L. Greer, M.D. Baró, Appl. Phys. Lett. 88 (2006) 171911.
[40] Y.J. Huang, J. Shen, Y.L. Chiu, J.J.J. Chen, J.F. Sun, Intermetallics 17 (2009) 190.
[41] A. Castellero, B. Moser, D.I. Uhlenhaut, F.H.D. Torre, Acta Mater. 56 (2008) 3777.
[42] F. Xu, Z.L. Long, X.H. Deng, P. Zhang, Nonferrous Met. Soc. China 23 (2013) 1646.
[43] J.C. Ye, J. Lu, C.T. Liu, Q. Wang, Y. Yang, Nat. Mater. 9 (2010) 619.
[44] H.B. Ke, P. Wen, H.L. Peng, W.H. Wang, A.L. Greer, Scr. Mater. 64 (2011) 966.